communications biology

A Nature Portfolio journal

Article

https://doi.org/10.1038/s42003-025-08938-4

Pyroglutamation of cell surface proteins CD47 and TRP1 by glutaminyl cyclase modulates therapeutic antibody binding

Anneloes van der Plas - van Duijn[1,2], Levi M. T. Winkelman[3], Claire Lensen[1], Maaike van Duivendijk[1], Ian Derksen[1], Jacqueline M. F. van Veenendaal[1], Gaby Schaap[2], Marjolein Sluijter[2], Tim J. B. van Groningen[1], Remco van Doorn[1], Thorbald van Hall[2], Roderick C. Slieker[1,2], Thomas H. Sharp[4], Joost B. Beltman[3], Kaspar Bresser[5] & Ferenc. A. Scheeren[1] ✉

Monoclonal antibodies are important modalities in the treatment of cancer. Post-translational modifications of proteins, such as glycosylation, can affect the binding affinity of therapeutic antibodies. Whether other PTMs modulate therapeutic antibody binding to different surface proteins is currently underexplored. Pyroglutamation is the post-translational cyclization of an N-terminal glutamine or glutamic acid residue into a pyroglutamate by glutaminyl cyclase. In this study, we investigated the impact of pyroglutamation on the binding affinity of three therapeutic antibodies targeting CD47 and TRP1. Here, we show that pyroglutamation on CD47 and TRP1 modulates the binding of anti(α)-CD47 magrolimab and αTRP1 TA99 and flanvotumab. Furthermore, the N-terminal glutamine on CD47 is crucial for effective antibody recognition, while pyroglutamation of TRP1 is involved in trafficking to the cell surface. These findings highlight that the pyroglutamation by glutaminyl cyclase can modulate the binding affinity of antibodies with therapeutic potential.

Monoclonal antibodies play a pivotal role in the first- and second-line treatment of various cancers, demonstrating significant efficacy in subsets of patients[1]. Despite the approval of multiple monoclonal antibodies as standard of care therapy, there remains an urgent need to identify other therapeutic targets to improve outcomes across diverse patient populations. Consequently, numerous antibodies have undergone clinical evaluation, including anti-(α)CD47 magrolimab and α-tyrosinase-related protein 1 (TRP1) targeting antibodies, such as clone TA99 and flanvotumab.

CD47, a ubiquitously expressed protein that can be overexpressed on the membranes of cancer cells, engages SIRPα on myeloid cells to initiate an inhibitory signaling cascade to suppress myeloid functions, such as phagocytosis and trogoptosis[2–6]. Magrolimab, a CD47-blocking antibody, disrupts this interaction, effectively alleviating this inhibitory immune checkpoint. Clinical trials of magrolimab combined with rituximab demonstrated promising response rates in patients with advanced lymphoma, as well as partial responses in ovarian and fallopian tube cancers[7,8]. However, recent clinical evaluations of magrolimab were terminated due to toxicities, including the ENHANCE studies (www.clinicaltrials.gov identifier NCT05079230), highlighting the need to investigate the mechanisms underlying the binding characteristics of magrolimab.

Beyond CD47, TRP1 has also emerged as a promising target for antibody-based therapies. TRP1 is a melanoma-associated antigen highly expressed on the surface of tumor cells in a subset of melanoma patients[9]. While its exact role in melanoma remains unclear, therapeutic antibodies such as αTRP1 clone TA99 and flanvotumab have been developed to target this marker due to the cell-type selective expression of TRP1 on the cell surface. Moreover, these antibodies have been tested as monotherapy or a component of CAR-T cells or bispecific T cell engagers[10–14]. αTRP1 clone TA99 was in a clinical phase 1 trial for metastatic melanoma in a T cell engaging format[12]. Early-phase clinical trials demonstrated encouraging responses, with one complete response and 37% of patients achieving stable disease upon flanvotumab treatment[13]. Factors that influence the binding affinity of these antibodies have been underexplored, including post-translational modifications (PTMs) on their cell surface target protein.

PTMs are enzymatic modifications that occur after protein translation and can influence protein structure, function, localization, stability, and receptor-ligand interactions[15–18]. For example, glycosylation, i.e. the addition

[1]Department of Dermatology, Leiden University Medical Center, Leiden, the Netherlands. [2]Department of Medical Oncology, Oncode institute, Leiden University Medical Center, Leiden, the Netherlands. [3]Division of Cell Systems and Drug Safety, Leiden Academic Centre for Drug Research, Leiden University, Leiden, the Netherlands. [4]School of Biochemistry, University of Bristol, Bristol, United Kingdom. [5]T Cell Differentiation Lab, Department of Research, Sanquin Blood Supply Foundation, Amsterdam, the Netherlands. ✉e-mail: f.a.scheeren@lumc.nl

of sugar moieties, can modulate therapeutic antibody affinity against immune checkpoints PD-1 and PD-L1[15,17,19–23]. Specifically, clinically approved αPD-1 antibodies camrelizumab and cemiplimab recognize the fucose of an N-glycan on PD-1[20,21]. Antibodies in clinical development, such as STM108, specifically target glycosylated PD-L1[15]. These examples underscore the therapeutic relevance of PTMs on target proteins in relation to the affinity of therapeutic antibodies. Based on these insights, we set out to determine whether pyroglutamation, a PTM, can modulate the binding affinity of other monoclonal antibodies.

Pyroglutamation is the enzymatic conversion of an N-terminal glutamine or glutamic acid residue into a pyroglutamate (pGlu) by glutaminyl cyclase enzymes QPCT and/or QPCTL. This PTM enhances protein stability and function[24–31]. For example, pyroglutamation can facilitate the binding of CD47 to SIRPα, enhance the activity of chemokines such as CCL2, influence the recognition of butyrophilins by γδ-T cells, and promote the pathogenicity of Aβ peptides involved in Alzheimer's disease[27–32]. In this study, we investigated the role of pyroglutamation on the binding affinity of therapeutic antibodies, including magrolimab and TRP1-targeting antibodies. Importantly, the targets of these antibodies, CD47 and TRP1, contain a conserved N-terminal glutamine after the signal peptide that acts as the substrate for glutaminyl cyclase. Our results reveal that glutaminyl cyclase activity and the presence of an N-terminal glutamine that can be modified into a pGlu can be critical for antibody binding. These findings underscore the importance of analyzing pyroglutamation to guide the development of optimized and differential therapeutics.

Results

Glutaminyl cyclase catalyzes the conversion of N-terminal glutamine or glutamic acid into pGlu. Here, we set out to determine whether the pGlu PTM plays a role in the recognition of antibodies which undergo clinical development. To identify target proteins, we first conducted an in silico prediction to identify proteins with an N-terminal glutamine or glutamic acid, following signal peptide cleavage. The 904 identified candidates were then cross-referenced with the Thera-SAbDab clinical antibody database to find clinically relevant antibodies targeting proteins with an N-terminal glutamine or glutamic acid (Sup. Data 1)[33]. We retrieved in total 37 protein targets with N-terminal glutamine or glutamic acid and we selected two protein targets with a conserved N-terminal glutamine for further analysis: CD47 and TRP1.

CD47 pyroglutamation is a key PTM for magrolimab and SIRPα binding

CD47 is a glycoprotein that contains a conserved N-terminal glutamine following its signal peptide, serving as the recognition site for the glutaminyl cyclase enzyme QPCTL (Sup. Fig. 1a)[29–31,34]. Pyroglutamation of CD47 by glutaminyl cyclase is essential for engagement of CD47 with SIRPα[29–31,34]. Given that SIRPα and magrolimab share a common binding site[34], we investigated whether glutaminyl cyclase activity modulates magrolimab binding to CD47.

First, we analyzed the previously established crystal structure of CD47 in conjunction with (i) the αCD47 clone B6H12.2, an antibody that binds CD47 independently of glutaminyl cyclase activity (pan-αCD47), (ii) recombinant human SIRPα-Fc, which requires pGlu on CD47 to bind (pGlu-specific), and (iii) magrolimab[31,34]. Whereas αCD47 clone B6H12.2 interacts with a region of CD47 distal from the pGlu-epitope, both SIRPα and magrolimab face the N-terminal pGlu-epitope present in the binding pocket of CD47, suggesting that pGlu formation may be involved in the binding of magrolimab to CD47 similar as to SIRPα (Fig. 1a).

To validate these findings, we used three human cell lines with high CD47 expression, including Burkitt's lymphoma cell line Daudi, melanoma cell line A375 and haploid cell line Hap1. These were selected based on the protein atlas and previous research[35]. QPCTL knockout (KO) lines were used and validated by flow cytometry (Fig. 1b, Sup. Fig. 1b for the gating strategy, and Sup. Fig. 1c). As expected, cells that were deficient for *QPCTL* exhibited reduced pGlu-specific human SIRPα-Fc and αCD47 clone CC2C6 staining intensities compared to wildtype cells, while the overall cell surface levels of CD47 as measured by pan-αCD47 clones B6H12 and 2D3 were not altered (Fig. 1b, Sup. Fig. 1c)[31]. Magrolimab binding was reduced fourfold in the absence of glutaminyl cyclase in Daudi cells based on the median fluorescent intensity (MFI; Fig. 1b). In addition, CD47 KO cells were generated to assess the specificity of magrolimab binding. CD47 deficient cells as verified by lack of pan-αCD47 clone 2D3 binding were unable to interact with magrolimab (Sup. Fig. 1d). These results indicate that QPCTL is required for optimal magrolimab engagement to CD47.

Next, we performed a titration of magrolimab on wildtype and QPCTL KO cell lines. Magrolimab attachment was reduced in the absence of QPCTL compared to wildtype cells in all three cell lines tested (Fig. 2a). The total levels of cell surface CD47 measured by pan-αCD47 clone 2D3 did not differ or were even slightly elevated in the QPCTL deficient cells (Fig. 2b), underscoring that transport of CD47 to the cell surface was not reduced by glutaminyl cyclase depletion.

Several small molecule inhibitors of glutaminyl cyclase have been developed, including PQ912 and SEN177. Given the potential and the current clinical assessment of glutaminyl cyclase inhibitors in patients with cancer (CTR20240727), we sought to validate our findings from the genetic KO cells using these glutaminyl cyclase inhibitors. All three cell lines were treated for three days with glutaminyl cyclase inhibitors and analyzed by flow cytometry upon antibody exposure. Similar to what was observed in the QPCTL KO cells, the pGlu-specific reagents SIRPα-Fc and αCD47 clone CC2C6 exhibited diminished binding upon glutaminyl cyclase inhibition without reducing the abundance of cell surface CD47 as measured with pan-αCD47 clone 2D3, validating the efficacy of the inhibitor (Sup. Fig. 2a). Magrolimab binding was also strongly and significantly reduced when glutaminyl cyclase activity was inhibited by PQ912 or SEN177 compared to the DMSO control in all three cell lines (Fig. 2c).

To investigate the necessity of the N-terminal glutamine for magrolimab binding on a molecular level, a CD47 mutant lacking this residue was transduced into Daudi cells deficient for CD47. Daudi cells expressing the CD47 mutant failed to engage with magrolimab, despite the surface expression of the mutant as confirmed by pan-αCD47 clone B6H12 staining (Fig. 2d, Sup. Fig. 2b). These findings collectively suggest that both glutaminyl cyclase activity and the presence of the N-terminal glutamine are crucial for magrolimab binding to CD47.

The binding affinity of magrolimab is decreased in the absence of glutaminyl cyclase activity as analyzed through mathematical modeling

To examine the differences in binding affinity of CD47 to magrolimab in wildtype and QPCTL KO cell lines, we developed a method in which we dynamically simulated the concentrations of antibody, ligand and antibody-ligand complex utilizing a system of ordinary differential equations (ODEs) while estimating K_D in the process (see Methods In silico K_D estimation and Fig. 3a for explanation of the approach). In brief, following estimation of the maximal MFI (MFI_{max}) from the data based on the highest nominal antibody concentrations (Fig. 3a, left panel), combinations of K_D and a factor that scales MFI values to concentrations of ligand-antibody complex are iteratively tried out to find optimal fits by simulating the associated equilibrium levels of the model variables (Fig. 3a, middle panel), and quantifying the resulting fit to the data (Fig. 3a, right panel). Application of this approach to artificial data closely mimicking the behavior of our experimental data (Sup. Fig. 3a) but with fixed known values for K_D, SF and MFI_{max} (Sup. Fig. 3b) showed that the resulting estimates were robustly retrieved for a range of parameter inputs (Sup. Fig. 3c-e). Next, we fitted our data of wildtype and QPCTL KO cells in this model to calculate the K_D values of magrolimab in both cell lines. QPCTL KO cells have higher K_D values compared to the wildtype cells (A375: 152 vs 74; Daudi: 60 vs 14; Hap1: 376 vs 9), indicative of a lower binding affinity of magrolimab to cells in the absence of glutaminyl cyclase activity (Fig. 3b). Importantly, we fitted two models to

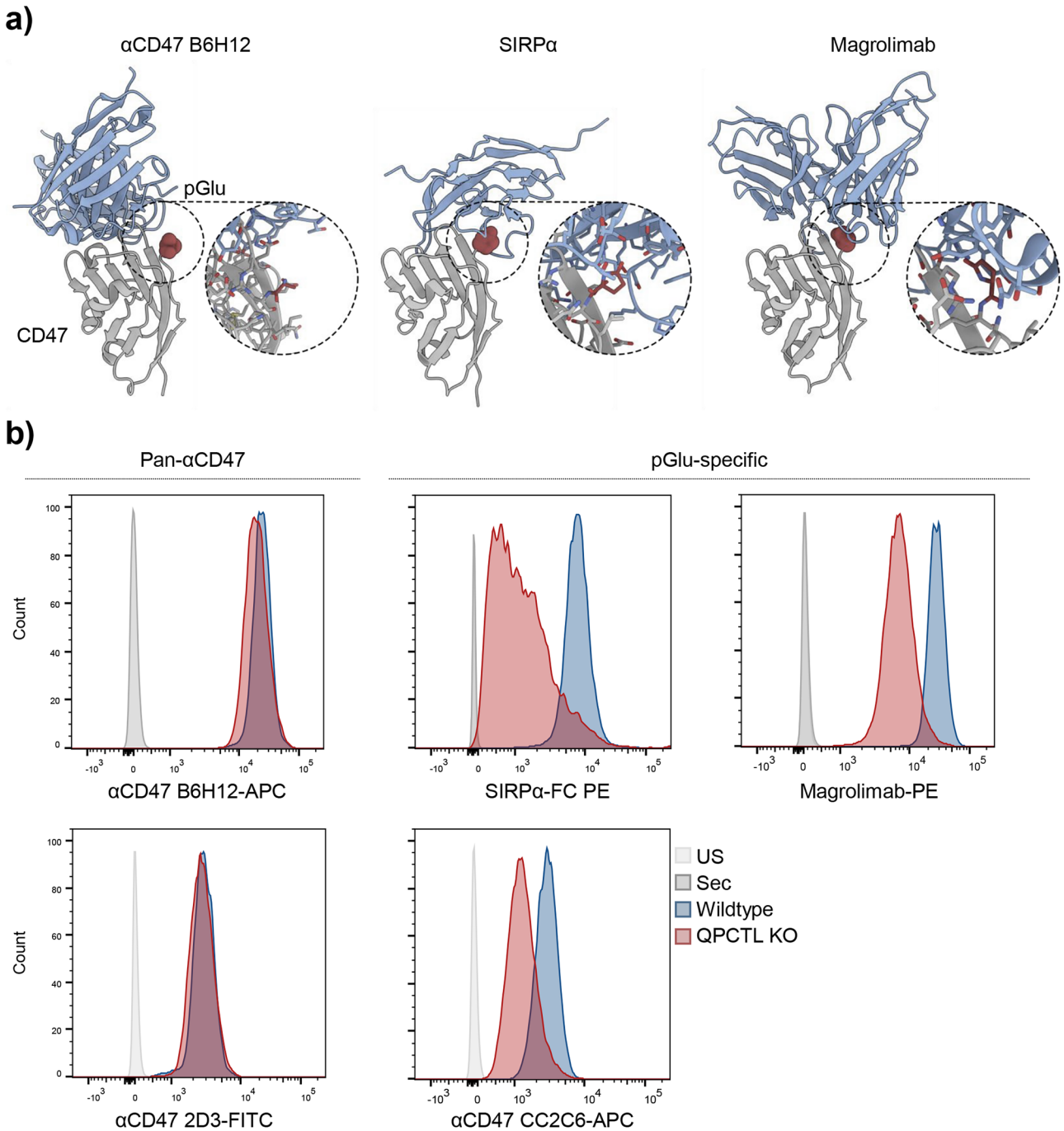

Fig. 1 | Magrolimab binding affinity is reduced in the absence of glutaminyl cyclase, while the cell surface expression levels of CD47 remained unaltered. **a** Crystal structures of αCD47 clone B6H12 (PDB: 5TZU), human SIRPα (PBD: 5IWL) or magrolimab (PBD: 2JJS, all in blue) with CD47 (gray). Red motif indicated the pGlu-epitope. **b** Representative histograms of pan-αCD47 antibodies clone B6H12 (1:50) followed by αmouse IgG APC (1:800), αCD47 clone 2D3 FITC (1:40), pGlu-specific recombinant human SIRPα-Fc (1:25) followed by αhuman clone M13 PE (1:100), αCD47 clone CC2C6 APC (1:10,000) and magrolimab (1:40,000) followed by αhuman clone QA19 PE (1:100), unstained (light gray) or secondary only (dark gray) staining on Daudi wildtype (blue) and QPCTL KO cells (red; n = 4). Abbreviations: pGlu, pyroglutamate; US, unstained; Sec, secondary antibody only; KO, knockout.

the data: a 'reduced model' in which we fitted a joint K_D value to both wildtype and QPCTL KO titration binding curves within a cell line (Sup. Fig. 3f), and a 'full model' in which we estimated separate K_D values for both curves (Fig. 3b). This analysis provided statistical evidence that the K_D values were indeed lower for wildtype than for KO cell lines (Akaike information criterion (AIC) values full versus reduced model: 612.4 vs 627.3 (Daudi), 539.2 vs 584.9 (Hap1), 664.7 vs 677.2 (A375).Together these results indicate that the binding affinity of magrolimab to CD47 is decreased in the absence of pGlu.

TRP1 pyroglutamation is a key PTM for αTRP1 clone TA99 and flanvotumab binding

TRP1 is a cell surface protein similar to CD47 in that it contains a conserved N-terminal glutamine following its signal peptide and a target for clinically explored antibody-based therapies (Sup. Fig. 4a). This led us to investigate whether glutaminyl cyclase plays a role in the binding affinity of antibodies αTRP1 clone TA99 and flanvotumab which both target TRP1 and have been undergoing clinical testing in different formats[10–13]. First, we used the previously established TRP1 crystal structure, and highlighted the pGlu-epitope

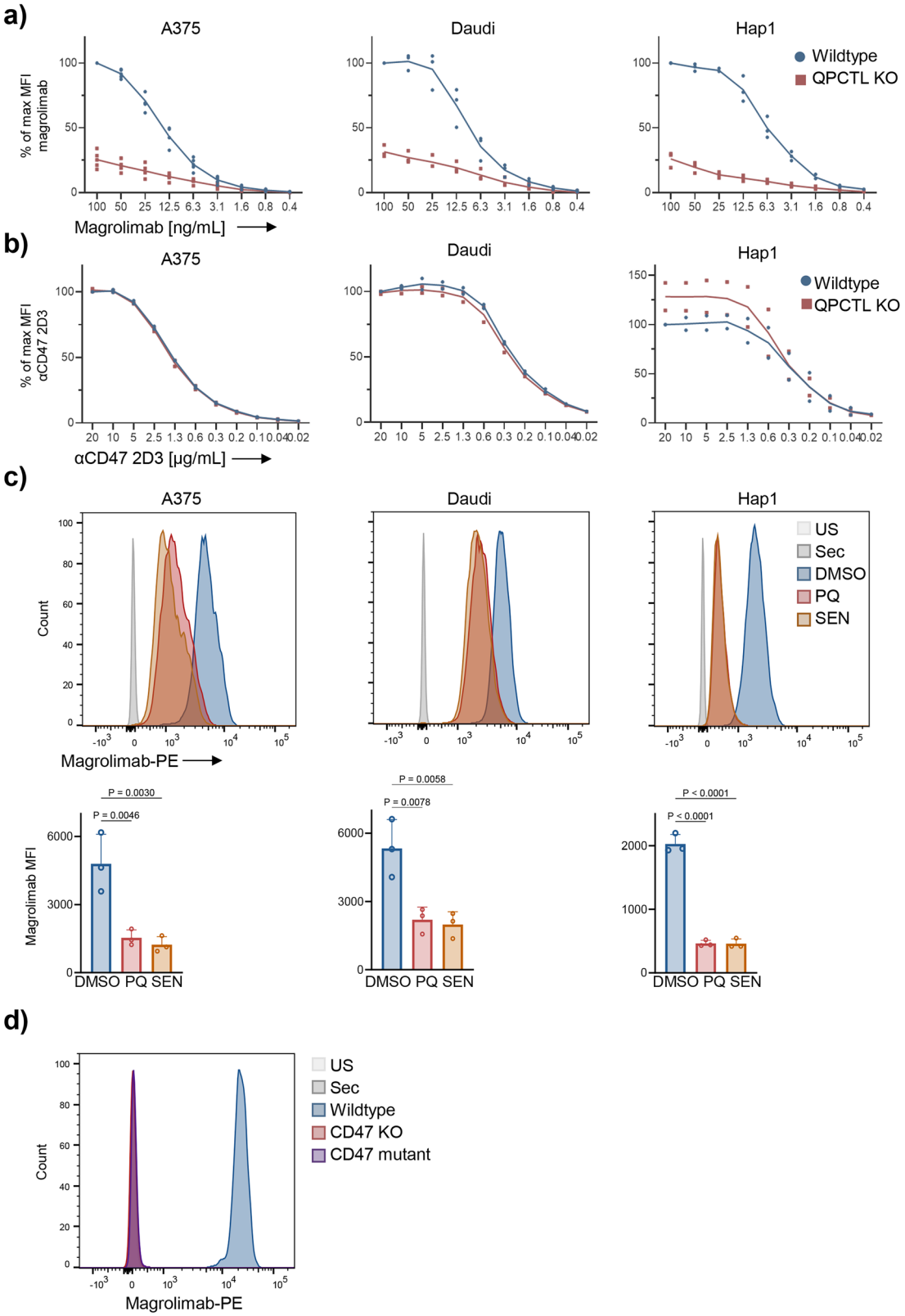

(Fig. 4a). Since both antibodies are cross-reactive between humans and mice[10], we tested our hypothesis using murine B16F10 melanoma cells that also express CD47 and require glutaminyl cyclase-modified CD47 in order to bind to mouse SIRPα[36]. Titrations of αTRP1 clone TA99 on B16F10 wildtype and QPCTL KO cells showed that the maximal binding of αTRP1 clone TA99 was strongly reduced upon QPCTL loss (Fig. 4b). Flanvotumab binding was similarly affected in QPCTL deficient B16F10 cells (Fig. 4c). These cells were verified using pGlu-specific recombinant mouse SIRPα-Fc and pan-αmouse CD47 clone MIAP301 (Sup. Fig. 4b). To verify whether αTRP1 clone TA99 and flanvotumab specifically recognized TRP1, the TRP1-negative pancreatic cancer cell line KPC-3 was transduced with a TRP1 plasmid, leading to its overexpression. KPC-3 cells that overexpress

Fig. 2 | Glutaminyl cyclase is involved in the binding of magrolimab to cancer cell lines. a Titration of magrolimab (1:1 dilution, commencing at 100 ng/mL) followed by αhuman IgG clone QA19 PE (1:100) on A375, Daudi and Hap1 wildtype (blue) and QPCTL KO (red) cells. Data represents individual data point and the line is the mean percentage of MFI of magrolimab staining relative to the MFI of 100 ng/mL magrolimab on wildtype cells (n ≥ 3). **b** Titration of αCD47 clone 2D3 (1:1 dilution, commencing at 20 µg/mL) on A375, Daudi and Hap1 wildtype (blue) and QPCTL KO (red) cells. Data represents individual data point and the line is the mean percentage of MFI of αCD47 clone 2D3 staining relative to the MFI of 20 µg/mL αCD47 clone 2D3 on wildtype cells (n = 2). **c** Representative histograms of magrolimab (1:40,000) followed by αhuman clone QA19 PE (1:100), unstained (gray) or αhuman clone QA19 PE only (dark gray) staining on A375, Daudi and Hap1 cells treated with 10 µM glutaminyl cyclase inhibitors PQ912 (red) or SEN177 (orange) or equal amounts of DMSO (blue) for three days. Bar graphs show the mean MFI of magrolimab, + standard deviation error bar (n = 3). One-way Anova was performed followed by the Dunnett's multiple comparisons test. **d** Representative histograms of magrolimab (1:40,000) followed by αhuman clone QA19 PE (1:100), unstained (gray) or αhuman clone QA19 only (dark gray) staining on Daudi wild-type (blue), CD47 KO (red) and CD47 KO cells transduced with the CD47 mutant (purple; n = 3). Abbreviations: MFI, median fluorescent intensity; KO, knockout; US, unstained; Sec, secondary antibody only; PQ, PQ912; SEN, SEN177.

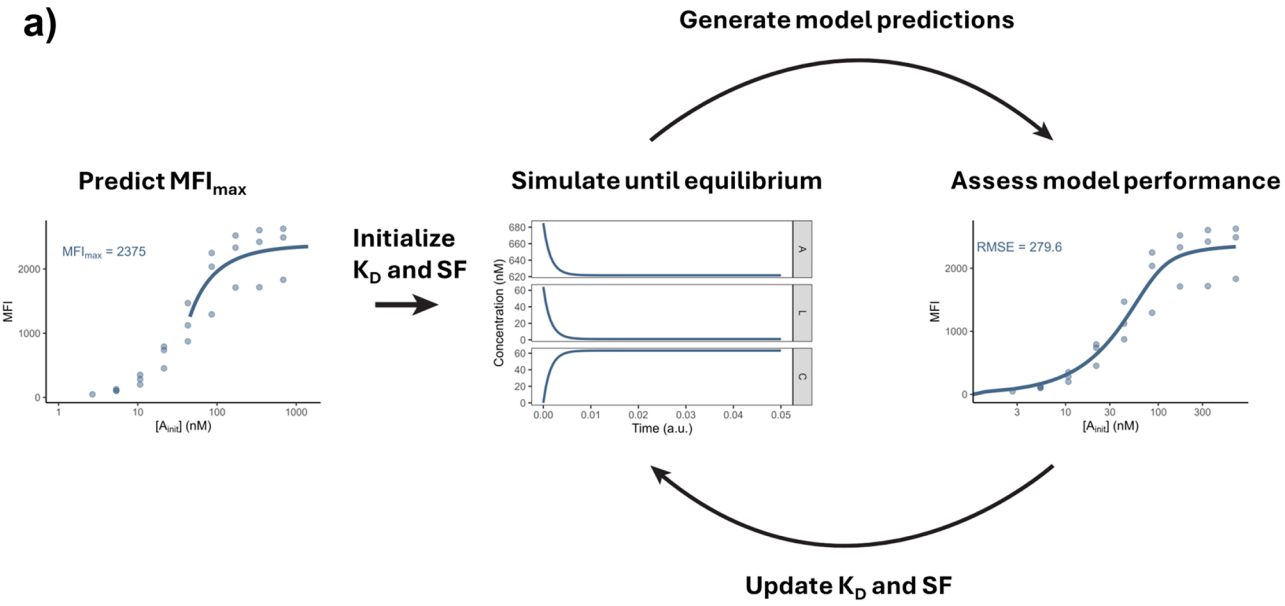

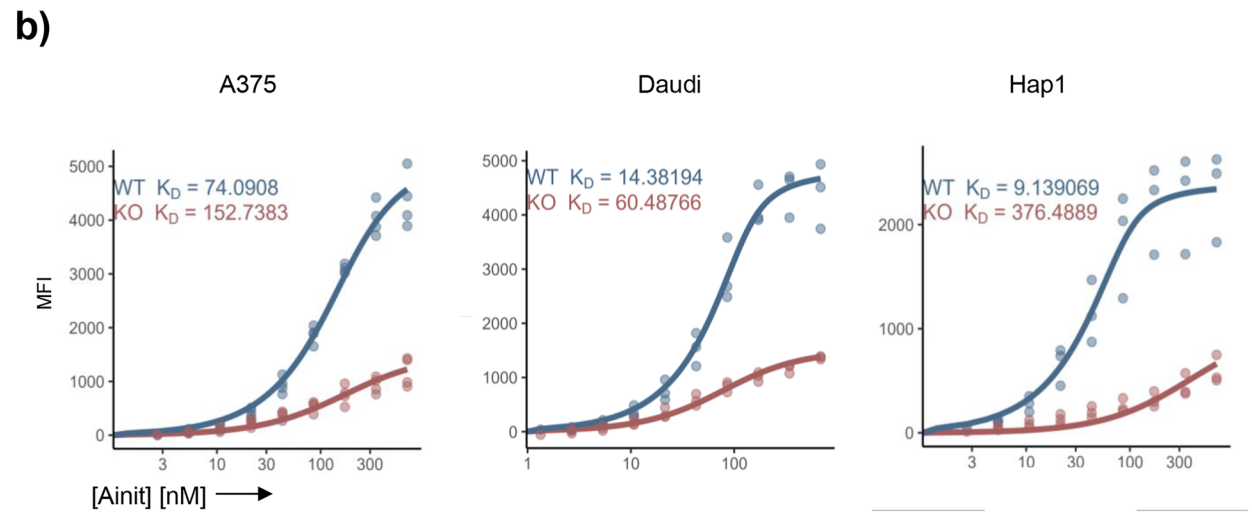

Fig. 3 | Dynamic modeling approach reveals that QPCTL increases binding affinity of CD47 to magrolimab. a Explanation of setup of model to determine K_D value. L_{init} is estimated through fitting MFI_{max} and dividing this value by SF (left panel). Initial values for A, L and C are used to predict their respective values at equilibrium for a given set of k_1 and k_2 (middle panel). Predicted [C] at equilibrium from (B) is multiplied by SF to obtain predicted MFI values that can be validated against observed values of MFI from experimental data (right panel). After model evaluation, K_D and SF are re-estimated, and simulations are re-run until residual deviance is minimal. **b** ODE model fit for titration binding curves of wildtype and KO conditions across three CD47 expressing cell lines utilizing the full model in which K_D values are estimated separately with indicated K_D values. Abbreviations: MFI, median fluorescent intensity; A, antibody; L, ligand; C, Complex; KO, knockout; ODE, ordinary differential equations; SF, scaling factor; RMSE; root mean squared error, WT, wildtype.

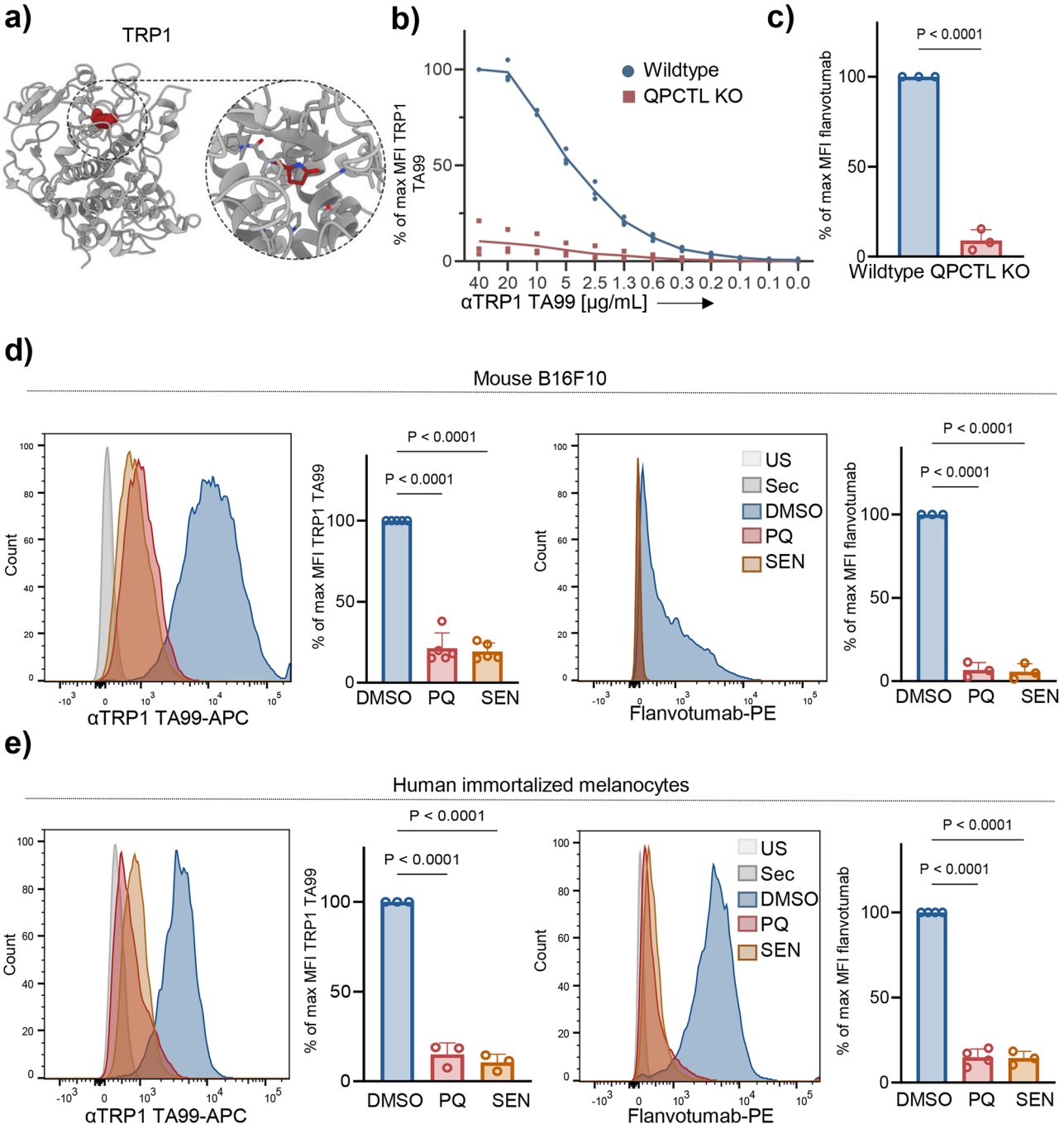

Fig. 4 | Glutaminyl cyclase is involved in the binding of αTRP1 clone TA99 and flanvotumab to melanoma cell lines. a Crystal structure of human TRP1 (PDB: 5M8L), with the red motif indicating the N-terminal pGlu. **b** Titration of αTRP1 clone TA99 (1:1 dilution, commencing at 40 µg/mL) followed by αmouse IgG APC (1:800) on murine B16F10 wildtype (blue) and QPCTL KO (red) cells. Data represents individual data point and the line is the mean percentage of MFI of αTRP1 clone TA99 staining relative to the MFI of 40 µg/mL αTRP1 clone TA99 on wildtype cells (n = 3). **c** Flanvotumab (1:200) followed by αhuman clone QA19 (1:100) on B16F10 wildtype (blue) and QPCTL KO (red) cells. Data represents the percentage of MFI, + standard deviation error, bar of flanvotumab staining relative to the MFI flanvotumab on wildtype cells. One-way Anova was performed followed by the Dunnett's multiple comparisons test (n = 3). **d** Representative histograms of αTRP1 clone TA99 (1:100) followed by αmouse IgG APC (1:800) or flanvotumab (1:200) followed by αhuman clone QA19 PE (1:100), unstained (gray) or secondary controls (dark gray) staining on B16F10 treated with 10 µM glutaminyl cyclase inhibitors PQ912 (red) or SEN177 (orange) or equal amounts of DMSO (blue) for three days. Bar graphs show the percentage of the MFI of αTRP1 clone TA99 or flanvotumab staining, + standard deviation error bar, relative to the MFI of DMSO control cells. One-way Anova was performed followed by the Dunnett's multiple comparisons test (n = 3). **e** Representative histograms of αTRP1 clone TA99 (1:100) followed by αmouse IgG APC (1:800), or flanvotumab (1:50) followed by αhuman clone QA19 PE (1:100), unstained (gray) or secondary controls (dark gray) staining on primary immortalized human melanocytes treated with 10 µM glutaminyl cyclase inhibitors PQ912 (red) or SEN177 (orange) or equal amounts of DMSO (blue) for three days. Bar graphs show the percentage of the MFI of αTRP1 clone TA99 or flanvotumab, + standard deviation error bar, relative to the MFI of DMSO control cells. One-way Anova was performed followed by the Dunnett's multiple comparisons test (n ≥ 3). Abbreviations: MFI, median fluorescent intensity; KO, knockout; US, unstained; Sec, secondary antibody only; PQ, PQ912; SEN, SEN177.

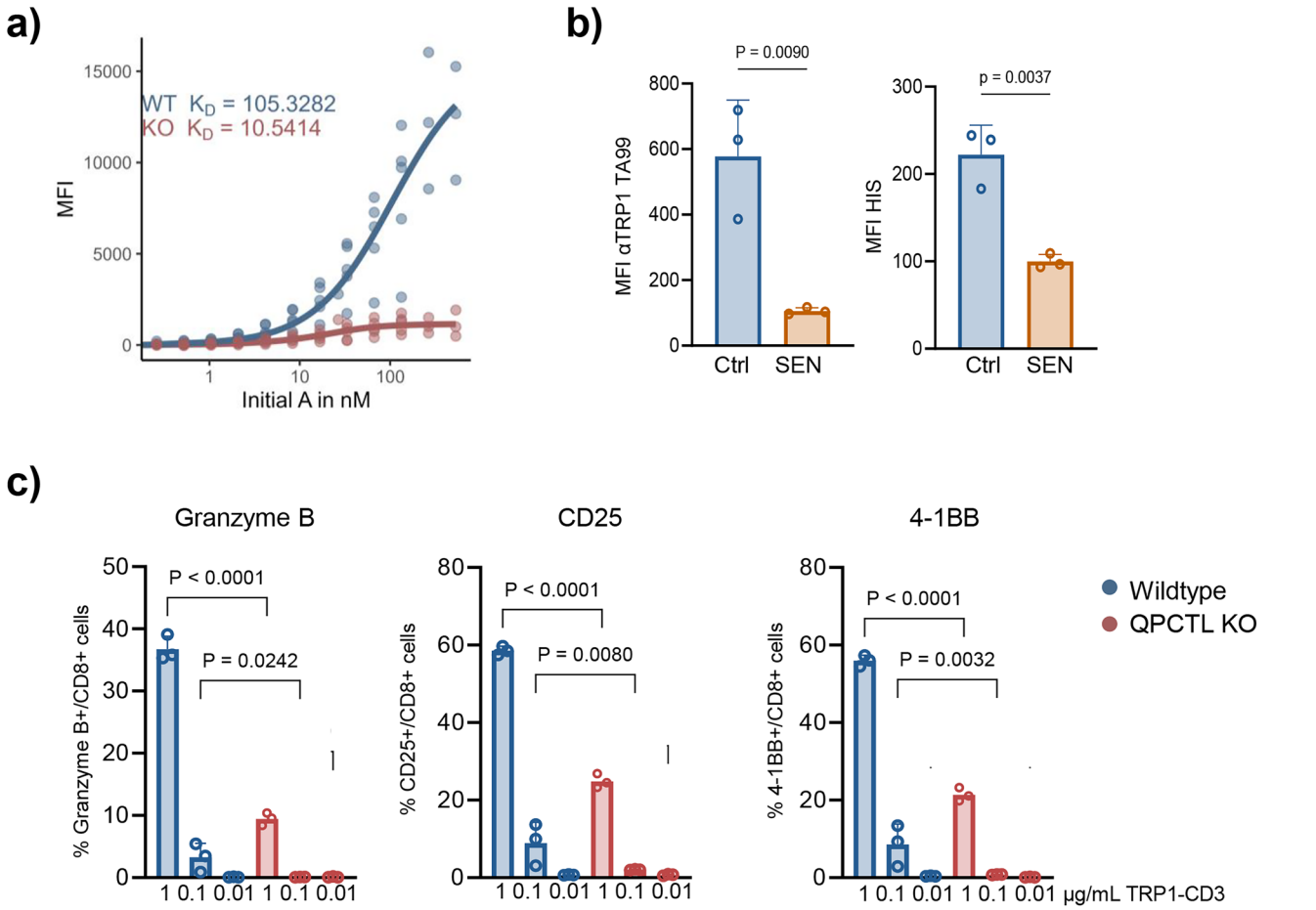

Fig. 5 | Glutaminyl cyclase is involved in the trafficking of TRP1 to the cell surface which affects TRP-CD3-bispecific T cell therapy. a K_D calculation of TRP1 TA99 on B16F10 wildtype and QPCTL KO cells. ODE model fit for titration binding curves of WT and QPCTL KO conditions for the B16F10 cell line utilizing the full model in which K_D values are estimated separately. **b** MFI of αTRP1 clone TA99 (1:50) followed by αmouse IgG APC (1:100) or αHIS PE (1:50) on grazoprevir treated HeLa cells expressing CAR-TRP1 in the presence or absence of 4 day treatment of 30 μM SEN177. Data represents the MFI, + standard deviation error bar. Unpaired T test was performed to assess the two groups (n = 3). **c** Percentage of CD8 + T-cells positive for the indicated markers that have been cocultured with B16F10 wildtype or QPCTL KO cells in the presence of 1, 0.1 or 0.01 ug/mL TRP1 TA99-CD3-bispecific antibody for 48 hours. Data represents the percentage, + standard deviation error bar. One-way Anova was performed to assess the groups (n = 3). Abbreviations: MFI, median fluorescent intensity; WT, wildtype; KO, knockout; PQ, PQ912; SEN, SEN177.

TRP1 were engaged by both αTRP1 clone TA99 and flanvotumab, while no staining was observed on the wildtype cells (Sup. Fig. 4c). Pharmacological inhibition of glutaminyl cyclase using PQ912 or SEN177 resulted in a strong and significant reduction of αTRP1 clone TA99 and flanvotumab attachment compared to the B16F10 DMSO control group (Fig. 4d). Diminished mouse SIRPα-Fc binding upon glutaminyl cyclase inhibition verified the efficacy of the inhibitor (Sup. Fig. 4d).

To determine the effects on human cells, we used primary immortalized melanocytes. First, we confirmed that untreated primary immortalized melanocytes express TRP1 on the surface as both αTRP1 clone TA99 and flanvotumab were able to bind the cells (Fig. 4e). Next, the cells were treated with the two glutaminyl cyclase inhibitors separately. Similarly to murine melanoma cells, αTRP1 clone TA99 and flanvotumab binding were diminished in primary immortalized melanocytes subjected to pharmacological inhibition of glutaminyl cyclase activity compared to DMSO-treated melanocytes (Fig. 4e, Sup. Fig. 4e). Additionally, SK-MEL-19, a human melanoma cell line, exhibited a similar reduction of αTRP1 clone TA99 binding in the absence of glutaminyl cyclase activity (Sup. Fig. 4f).

We then applied our in-silico modeling to determine K_D values related to the binding of αTRP1 clone TA99 to TRP1 in wildtype and QPCTL KO B16F10 cells. We found lower K_D values for QPCTL KO cells compared to their wildtype counterparts (11 vs 105), indicating that αTRP1 clone TA99 binding affinity to TRP1 is reduced upon pyroglutamation (Fig. 5a, Sup. Fig. 3f right panel). Fitting the data to the full and reduced models, we found that these K_D values were statistically different between the groups (AIC value full vs reduce model: 1585.1 vs 1587). These findings may be explained by an overall decreased transport of TRP1 to the cell surface in the absence of the pyroglutamation. To investigate this hypothesis, we designed a TRP1-CAR-construct that contained an HIS tag as a proxy for the total levels of the recombinant TRP1 on the cell surface as we did not obtain an antibody that bound extracellular TRP1 independent of QPCTL activity[37]. In the absence of glutaminyl cyclase, both αTRP1 clone TA99 and αHIS binding were reduced, indicating that the total levels of TRP1 on the cell surface were indeed diminished upon glutaminyl cyclase inhibition (Fig. 5b). In line with these results, no extracellular binding of αTRP1 TA99 was observed in HeLa cells overexpressing a TRP1 Q > A mutant while two antibodies against TRP1 were able to bind to the alanine mutant intracellularly (Sup. Fig. 4g). Thus, it appears that glutaminyl cyclase activity facilitates the trafficking of TRP1 to the cell surface and subsequent engagement with TRP1-binding antibodies.

To assess whether loss of TRP1 antibody binding has functional consequences for immune cell activation, we co-incubated B16F10 wildtype and QPCTL KO cells with mouse CD8 + T cells and subsequently stained these

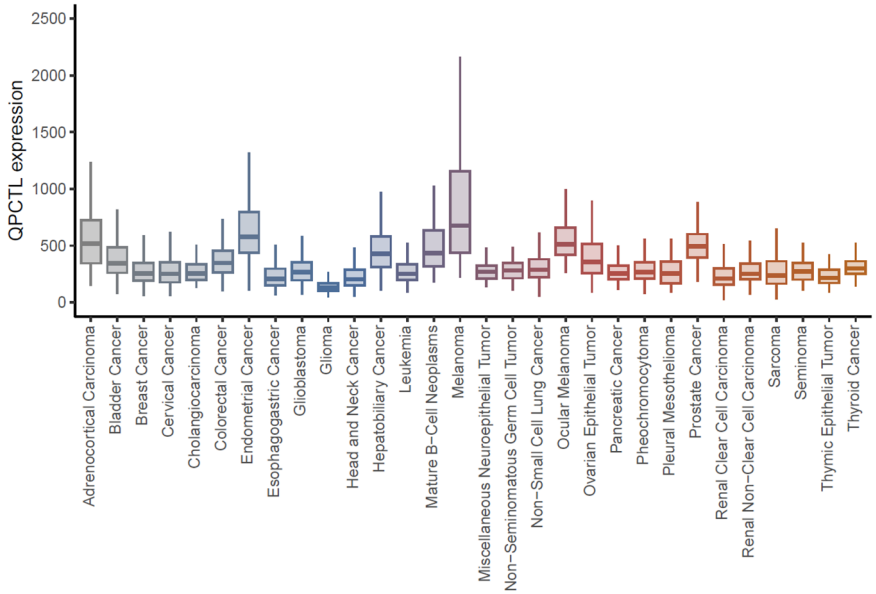

Fig. 6 | Glutaminyl cyclase RNA levels are differentially expressed between normal and tumor cells across cancer types. RNA-seq data (RSEM quantified, batch normalized) was obtained from TCGA for 30 tumor types for QPCTL.

cells for various T cell activation markers. The percentages of granzyme B, CD25 and 4-1BB in CD8 positive cells were all significantly lower in the T cells cocultured with the QPCTL KO cells compared to wildtype cells, indicative of less CD8 + T cell activation (Fig. 5c). To conclude, the absence of pGlu on TRP1 can lower the activation status of CD8 + T cells in the presence of a TRP1-bispecific T cell engager.

Glutaminyl cyclase is differentially regulated across and within tumor types

We next examined RNA expression of glutaminyl cyclase across patients and cancer types. Variation in enzyme expression could influence the amount of pyroglutamation and therefore may significantly impact the efficacy of antibody-based therapies. As has already been observed for glycosylation, differences in the expression of enzymes involved in the glycosylation pathway on PD-1/PD-L1 directly affect the binding affinity of specific therapeutic antibodies[15,17,19–23]. We compared the expression of QPCTL across 30 different cancer types (Fig. 6) using data obtained from The Cancer Genome Atlas (TCGA). QPCTL is expressed in all tumor types, albeit at varying levels. High expression of QPCTL occurs in cutaneous skin melanoma, whereas QPCTL is lowly expressed in a number of tumor types, including glioma and leukemia tumors. In addition, for some tumor types there is a large inter-patient variability of QPCTL RNA expression levels. These results suggest that QPCTL is differentially expressed between human cancer types and also variable across patients within the same cancer type. This variability could significantly influence the level of the N-terminal pGlu PTM, both across different cancer types and on an individual, personalized level, which will be explored in future work.

Discussion

PTMs have been described to influence protein structure and function, and glycosylation has been demonstrated to affect the interactions between clinically tested antibodies and their modified cell surface proteins, such as PD-1 and PD-L1[15,17,19–23]. In contrast, the effect of pyroglutamation, the cyclization of glutamine or glutamic acid into pGlu by the enzyme family glutaminyl cyclase, has been underexplored, despite pyroglutamation impacting the structure, activity, and stability of membrane and secreted proteins, as well as their protein engagement[27–31]. Here, we assessed whether pyroglutamation influenced clinically evaluated αCD47 magrolimab binding to CD47 and αTRP1 clone TA99 and flanvotumab binding to TRP1, as both target proteins contain an N-terminal glutamine that act as the recognition site for glutaminyl cyclase.

Our findings reveal that the PTM pyroglutamation on the antigen has the potency to significantly impact antibody binding affinity with consequences for antibody effector functions as shown with a bispecific T cell engager. We demonstrated the dependence of magrolimab on glutaminyl cyclase activity using genetic and pharmacological inhibition assays. Consistent with prior reports, reduced magrolimab engagement was observed following treatment with glutaminyl cyclase inhibitors[38]. Since the pGlu epitope on CD47 is located in the binding pocket for SIRPα, its absence can affect blocking antibody binding affinity. It is currently unknown whether the modification is part of the recognized epitope or a conformational change of the protein diminishes antibody binding. Future studies should evaluate if other CD47-targeting compounds also depend on this PTM, such as ligufalimab and evorpacept[39].

We extended these findings to TRP1, for which the binding affinity with αTRP1 clone TA99 as estimated through fitting our mathematical model to the flow cytometry data was actually stronger in the absence of glutaminyl cyclase activity than in its presence, i.e., the effect of pyroglutamation on the binding affinity was opposite to the CD47-magrolimab interaction. Our finding that binding to the αTRP1 antibodies was nevertheless almost absent without glutaminyl cyclase activity can likely be explained by lower levels of TRP1 on the cell surface. These dependencies on pyroglutamation highlights potential vulnerabilities of TRP1-targeting therapies to variable glutaminyl cyclase expression, such as clinically assessed flanvotumab-based CAR-T cells and the αTRP1 clone TA99-based bispecific T cell engager (NCT04551352)[11,12]. In addition, αTRP1 clone TA99 is often used as a melanoma-opsonizing antibody in combination with CD47 blockade[40–42]. Considering that glutaminyl cyclase inhibitors are currently being investigated in an early phase clinical trial in cancer (CTR20240727)[40–42], caution should be warranted to combine glutaminyl cyclase inhibitors with TRP1-opsonizing antibodies, as the decreased binding of the latter may hamper the efficacy of the combination treatment.

Recently, we have identified a functional role in the mosquito immune response for the protease-cleaved and pyroglutamated form of the circumsporozoite Protein (CSP) in *P. falciparum*, the parasite responsible for malaria[43]. Importantly, pGlu-specific antibodies targeting pyroglutamated CSP have been isolated from malaria-infected individuals that exhibit neutralizing capabilities at the liver stage in a human liver-chimeric mouse model. These findings highlight the clinical potential of pGlu-specific antibodies[44]. In addition, Donanemab is an FDA-approved antibody therapy that selectively binds to pGlu-modified Aβ peptides in patients with

Alzheimer's disease[32], and αCD3ε-engaging antibody hE10 also recognized the pyroglutamate on CD3ε[45]. These findings underscore the clinical relevance of this type of PTM in antibody-based therapies. Whether therapeutic antibodies against other N-terminal glutamine or glutamic acid containing peptides or proteins are modulated by glutaminyl cyclase remains undetermined.

This study provides valuable insights but has limitations. First of all, spontaneous conversion of glutamine can occur in vitro and is affected by factors such as pH, temperature and certain buffer components[46–48]. We did not, however, detect an increase in SIRPα binding in the QPCTL KO cells over time nor did others find detectable levels of spontaneous pGlu formation on CD47[31]. Given that spontaneous formation of pyroglutamate from glutamine takes multiple days under physiological conditions[46], it is unlikely that our glutaminyl inhibition data are significantly confounded by spontaneous levels of pyroglutamation. Whether pyroglutamation of CD47 and TRP1 in humans in vivo is fully dependent on glutaminyl cyclase activity remains undetermined and should be further explored in the context of therapeutic antibody binding.

Second, the detection of an N-terminal pGlu is challenging as spontaneous modifications can occur during sample preparation for mass spectrometry analysis, which complicates identification of enzymatic-induced pGlu modification[46]. While prior research demonstrated the pGlu modification using one-dimensional isoelectric focusing[31], this study used an indirect approach via recombinant SIRPα binding.

Variability in QPCTL expression across different cancer types suggests differential impact on antibody therapy. For example, QPCTL is highly expressed in melanoma but lowly expressed in glioma and leukemia. Additionally, we observed inter-patient variability. Future research is warranted to investigate the role of glutaminyl cyclase activity and the pyroglutamation-status on therapeutic antibody efficacy, which may lead to improved therapeutic design and potentially patient selection for antibody-based therapy.

In conclusion, our study highlights the crucial role of pyroglutamation in modulating antibody binding to CD47 and TRP1, underlining the importance of assessing PTMs on target proteins for antibody therapy. Future research should investigate whether glutaminyl cyclase expression predicts antibody efficacy, paving the way for improved and differentiated PTM antibody therapies.

Materials and Methods

Cell culture

Human melanoma cell line A375, cervical cancer cell line HeLa, human embryonic kidney cell line HEK293T (#CRL-3216, ATCC) were maintained in DMEM, Burkitt's lymphoma cell line Daudi and haploid cell line Hap1 in IMDM (#12440-053, Gibco) and melanoma line SK-MEL-19 in RPMI (#22409-015, Gibco). Murine melanoma cell line B16F10 and pancreatic ductal adenocarcinoma cell line KPC-3 were cultured in DMEM (#10938-025, Gibco). All media was supplemented with 8% FCS and 1x Penicillin-Streptomycin-L-Glutamine mix (#10378016, Gibco). Primary hTERT immortalized melanocytes were cultured in D254 medium (#M254500, ThermoFisher Scientific) supplemented with HMGSII (#S0165, ThermoFisher Scientific) and Penicillin-Streptomycin. Cells were regularly checked for the absence of mycoplasma infection. HeLa was kindly gifted by the department of Cell and Chemical Biology, LUMC, Daudi, B16F10 and SK-MEL-19 from the department of Medical Oncology, LUMC, A375 and Hap1 from rof. Dr. T.R. brummelkamp and Prof T.N. Schumacher, Netherland Cancer Institute[31], and the immortalized melanocytes from the group of Remco van Doorn, Department of Dermatology, LUMC. For glutaminyl cyclase inhibitions, cells were seeded in a 6-wells plate and treated with 10 μM PQ912 (#T22403, TargetMol) or SEN177 (#SML1615, Sigma) or equal amounts of DMSO for three days, which was supplemented to the medium daily. For the secreting TRP-expressing cells, cells were seeded in a T25 flask and cultured for 4 days with 30 μM SEN177 or DMSO in the presence or absence of 6 μM grazoprevir which were both supplemented daily.

CRISPR/Cas9

A375 QPCTL KO cells and Hap1 CD47 and QPCTL KO were generated by Logtenberg et al. as previously described[31]. KPC-3 wildtype and TRP1 overexpressing cells were kindly gifted by Thorbald Hall's group[49].sgRNA targeting human CD47 (CAGCAACAGCGCCGCTACCA), human QPCTL (CCGGGGTTCGCACAACCAGC), mouse QPCTL (CGGCAGCGGCTCGAGGATCG) were cloned into PX459 V2 vector (#62988, Addgene). For adherent cell line B16F10, cells were seeded and the next day transfected with 5 μL lipofectamine (#11668027, ThermoFisher Scientific). 2 μg/mL puromycin (#ant-pr-1, Invivogen) was used to select the transfected cells, which was removed after two days. Serial dilutions at 0.3 cells/well in a 96 wells-plate were conducted to generate clonal KO cell lines, which were verified by flow cytometry. For suspension cell line Daudi, transfection was obtained through electroporation using the Nucleofector TM I/II/2b Kit (#VCA-1003, Lonza). After one day of recovery, transfected cells were selected with 1 μg/mL puromycin for Daudi cells. After multiple rounds of sorting to obtain a high purity population of KO cells using αCD47 clone CC2C6 (1:10,000, #323124, Biolegend) on the SRT ML-I, -II CytoFLEX SRT Benchtop cell sorter (Beckman Coulter, Brea, CA, USA), bulk KO cells were validated and used for future experiments.

For lentiviral production, HEK293T cells were seeded and transfected with CD47-mutant[31], TRP1-CAR-construct (Addgene #242866), TRP1-overexpressing wildtype (Addgene #242867) or Q > A mutant (Addgene ##242868) and packaging plasmids pCMV-VSV-G (#8454, Addgene), pMDLg/pRRE (#12251, Addgene) and pRSV-Rev (#12253, Addgene) or together with 1 μg packaging plasmids Pax2 (#12260, Addgene) and 1 μg Pmd2 (#12259, Addgene, both gifted from Dr. D. Trono). The next day, medium was replenished. Medium was collected, spun down for 5 minutes at 2000 rpm and supernatant was collected for two consecutive days and meanwhile replenished. Target cells were transduced with this medium through 90 minutes centrifugation at 2000 rpm or direct supplementation to the medium and the next day selected with 1 μg/mL puromycin for Daudi cells or 2 μg/mL puromycin for HeLa cells for at least one week.

Flow cytometry

100,000 cells were stained for 30 minutes with αhuman CD47 clone B6H12 (1:50, #SC12730, Santa Cruz), αhuman CD47 clone 2D3 FITC (1:40, #11-0478-42, Invitrogen), αhuman CD47 clone CC2C6 APC (1:10,000, #323124, Biolegend), human SIRPA-Fc (1:25 or 1:50 of 0.1 μg/mL in PBS, #4546-SA, R&D), magrolimab (concentrations as indicated, #A2036, SelleckChem), αTRP1 clone TA99 (concentrations as indicated, #SC-58438, Santa Cruz), flanvotumab (concentrations as indicated, #MA5-41956, ThermoFisher), mouse SIRPα-FC (1:200 of 0.2 μg/mL in PBS, #7154-SA, R&D), αmouse CD47 clone MIAP301 APC (1:40, #17-0471-82, Invitrogen) or αHIS PE (1:50, clone J095G46, #362602, Biolegend) in a total volume of 50 μL facs buffer (1% FCS in PBS) on ice shielded from light. After two rounds of washing with excess facs buffer, cells were incubated with 50 μL facs buffer supplemented with goat-αmouse clone Poly4053 APC (1:800, #405308, Biolegend), rat-αhuman clone M1310G05 PE (M13, 1:100, #410708, Biolegend), or mouse-αhuman clone QA19A42 PE (QA19, 1:100, #366904, Biolegend) as further elaborated in the figure legends.

For intracellular staining, cells were fixed in 4% paraformaldehyde (#P6148, Sigma) and permeabilized in facs buffer supplemented with 0.1% saponin (#S7900, Sigma). Cells were incubated with polyclonal αTRP1 (1:100, #EPR13063, Abcam) or αTRP1 clone TA99 (1:100, #SC-58438, Santa Cruz), diluted in 50 μL facs buffer supplemented with saponin for 30 minutes on ice shielded from light. After two rounds of washing with excess facs buffer supplemented with saponin, cells were incubated with 50 μL facs/saponin buffer supplemented with goat-αrabbit clone Poly4064 PE (1:100, #405308, Biolegend) for polyclonal-αTRP1 or goat-αmouse clone Poly4053 APC (1:800, #405308, Biolegend) for αTRP1 TA99 for 30 minutes on ice shielded from light. Cells were analyzed after two rounds of extensive washing. Flow experiments were conducted on an LSR-II (BD FACS LSR-II 4 L Full, BD Biosciences, San Jose, CA, USA), a BD FACS LSRFortessa 4 L (BD Biosciences, San Jose, CA, USA) or a Sony ID7000 Spectral Cell

Analyzer (Sony Biotechnology Inc., San Jose, CA, USA) at the Flow cytometry Core Facility of the LUMC. Data was analyzed using FlowJo (V10.8).

Mice and coculture experiments

Two six to eight week old male C57BL/6 J mice were purchased from Charles River, The Netherlands, and housed at pathogen-free conditions in the animal facility of the LUMC. After one week of acclimatization, mice were euthanized and spleens and lymph nodes were collected. This study was approved by the Dutch animal ethics committee and the local Animal Welfare Body of the LUMC on permit number AVD11600202417735. This experiment was performed in accordance with the Dutch Act on Animal Experimentation. We have complied with all relevant ethical regulations for animal use. Next, 30,000 irradiated (6000 Rad) B16F10 wildtype and QPCTL KO cells were plated in a 96 wells plate, and cocultured with CD8 cells isolated and enriched from spleens and lymph nodes of C57B1/6 J mice in the presence of IL-7 (10 ng/mL) and various dilutions of CD3-TRP TA99-bispecific antibody (starting from 1 µg/mL, 1:10 dilutions, Absolute Antibody, #bAb0136,Mouse IgG2a mCD3e KIH bispecific, Fc Silent™, Kappa). After a coculture of 48 hours, the cells in suspension were collected and stained for granzyme-B Percp Cy5.5 (1:100, #372212, Biolegend), CD8 PE (1:800, #100708, Biolegend), CD25 BV421 (1:200, #102034, Biolegend) and CD137 APC (1:100, #106110, Biolegend) according to the flow cytometry protocols mentioned above.

In silico prediction and antibody selection

All human protein entries with the status "UniProtKB reviewed (Swiss-Prot)" were downloaded from UniProt (20,421 entries) in January 2025, in addition to annotations for initiator methionine's and signal peptides. Only experimentally observed initiator methionine's were included in this analysis. For signal peptide annotation, both experimentally validated and predicted signal peptides were included. Predicted signal peptides were only included if detected by 2 out of 4 prediction methods; Phobius, Predotar, SignalP and TargetP. Initiator methionine's and signal peptides with trimmed from the amino acid sequences, and proteins starting with either a glutamine (563 entries) or glutamic acid (341 entries) amino acid were selected. These predicted genes were cross-referenced to the Thera-SAbDab database to discover clinically relevant antibodies against glutamine or glutamic-acid bearing proteins[33].

In silico K_D estimation

Previous modeling studies have attempted a similar approach in which a titration binding curve is fitted using a Michaelis-Menten-like formula after which K_D was estimated as the EC50 of the fitted curve[50,51]. However, this approach is expected to give a poor prediction of K_D values when applied to typical titration binding data in which nominal antibody concentrations are coupled to an MFI reflecting antibody-ligand complex after having settled at equilibrium (Sup. Fig. 3g left panel; Sup. Methods). Rather than using nominal antibody concentrations, one should use equilibrium concentrations of unbound antibody (Sup. Fig. 3g right panel), yet these are not directly available.

In order to quantify the binding affinity of CD47 and TRP1 to magrolimab and TA99 respectively, we consider a straightforward model for binding kinetics represented in reaction scheme 1. This scheme states that an antibody together with a ligand can reversibly bind to form a complex:

$$[A] + [L] \rightleftharpoons [C] \quad (1)$$

Here, [A] is the concentration of antibody, [L] is the concentration of ligand, [C] is the concentration of complex and k1 and k2 are the rates of complex association and dissociation respectively.

In the above model, the ratio between k_2 and k_1 -commonly referred to as K_D - can be used to quantify the ligand's affinity to bind to the antibody. Although a measure of K_D can be determined accurately using Surface Plasmon Resonance (SPR)[52], the required equipment and consumables are costly. Several labs have therefore previously attempted to estimate a measure of K_D by applying mathematical modeling to flow cytometry data acquired at several antibody concentrations to bypass the need of SPR[50,51]. In these studies, the following Michaelis-Menten-like formula was utilized to describe the antibody-binding titration curves following from the MFI as a function of the antibody concentration:

$$MFI = \frac{MFI_{\max}[A]}{K_D + [A]} \quad (2)$$

Fitting such a curve requires the optimization of MFI_{max} and K_D, thus yielding a direct measure of binding affinity through the optimized K_D parameter. If we substitute [A] with K_D in Eq. 2 and simplify, we obtain: $MFI = MFI_{max}/2$. Thus, the EC50 - i.e., [A] yielding half maximal MFI - equals K_D which allows one to directly read off K_D from a (fitted) titration binding curve. One major caveat that was not accounted for in the previous studies however, is that Eq. 2 only follows from Eq. 1, if the entire system is at equilibrium (Supplementary methods).

Similar to previous modeling attempts[50,51], we used reaction scheme S1 as the basis for our approach to quantify antibody-ligand binding affinity. Our ODE based model describes the dynamic behavior of the concentrations of antibody, ligand and antibody-ligand complex (Eqs. 3, 4 and 5 respectively).

$$\frac{d[A]}{dt} = k_2[C] - k_1[A][L] \quad (3)$$

$$\frac{d[L]}{dt} = k_2[C] - k_1[A][L] \quad (4)$$

$$\frac{d[C]}{dt} = k_1[A][L] + k_2[C]. \quad (5)$$

We aimed to use this ODE model to predict [C] at equilibrium from the initial rather than the equilibrium concentration of the antibody, and estimate K_D in the process. The major challenge in this approach is that the initial concentration of ligand is not known. However, as reaction scheme S1 implies a molar equivalence of 1:1 between [L] and [A] (i.e., 1 antibody molecule binds to 1 ligand molecule, giving rise to 1 complex), the maximal attainable [C] should be equal to the initial [L] (because at infinitely high [A], all ligand is bound). We can therefore use the asymptote of the titration binding curve to estimate the initial concentration of [L] after accounting for a factor that scales MFI to a molar concentration of complex. Thus, estimating K_D requires determination of the MFI_{max} as well as this scaling factor (SF).

Although Eq. 2 is not suitable for K_D estimation from data pertaining to nominal concentrations of antibody and measurements of MFI at equilibrium, curves derived from directly applying such data to Eq. 2, have shown to yield relatively low deviance[50,51]. This suggests that the fitted estimate of MFI_{max} (using Eq. 2), representing the horizontal asymptote of the curve, could nonetheless be a good estimate of the true maximally attainable [C] based on data like in Fig. 2a.

In practice however, simulations of the ODE system with predetermined parameters and initial conditions, show that MFI_{max} is systematically overestimated when using this approach (Sup. Fig. 3h, j). This bias can largely be attributed to the fact that the Michaelis-Menten-like equation is not flexible enough to capture the abrupt saturation of MFI at high levels of initial [A] coupled with the more gradual increase in MFI at low levels of initial [A] (Sup. Fig. 3i). Fitting a more complex equation to predict MFImax from titration binding curves increases the risk of overfitting the data that (due to heteroscedasticity) can be relatively variable around the asymptote. Instead we opted to determine MFImax by restricting our fit of the Michaelis-Menten-like curve through five datapoints pertaining to the highest tested concentrations of antibody. This

approach greatly reduced bias across a wide range of theoretical K_D values (Sup. Fig. 3i, j).

From there, the fitting procedure continues as follows: The initial [L] is estimated as the MFI_{max} divided by an estimate of SF (Fig. 3a left panel). Because this renders corresponding values for the initial concentrations of antibody, ligand and complex, the ODE model can predict their values at equilibrium for any given pair of k1 and k2 (Fig. 3a middle panel). Since the equilibrium values of [A], [L], and [C] depend only on the ratio between k2 and k1 (i.e. K_D) and not on their magnitudes, one of the two parameters can be fixed while fitting the other. We arbitrarily decided to fix k1 to 1 which conveniently implies that the estimate of k2 directly reflects K_D. We then multiplied the simulated [C] at equilibrium with SF to obtain a predicted MFI for any initial [A], which we then compared to the observed MFI values to assess model performance (Fig. 3a right panel). In an iterative process, we performed this procedure numerous times in order to identify the values for SF and k2 that minimize the model's residual deviance using non-linear least squares regression.

Although the estimation of the K_D value of a ligand-antibody interaction from titration binding curves can be of great value in itself, the primary goal of this study was to statistically assess differences in binding affinity between ligands at the cell-surface of WT and QPCTL KO cell-lines, requiring an expansion of this technique. To this end, we fitted two models in which the WT and KO data for a given cell-type were fitted simultaneously. In the so-called 'full model', we estimated a joint SF to link the MFI values from KO and WT data to concentrations of ligand-antibody complex, whereas we fitted k2 separately for the KO and WT lines. In the so-called 'reduced model', we also constrained k2 to be shared across cell-lines. We assessed the performance of the two nested models in terms of the AIC to strike a balance between goodness-of-fit and model complexity. We considered the K_D values between WT and KO cell-lines to be different if the AIC of the full model was lower compared to that of the reduced model, indicating that the decrease in residual variance of the full model outweighed the penalty for introducing the added parameter.

Before applying this approach to the experimental data, we tested its validity by generating a large number of artificial data sets that closely mimicked the design and behavior of the experimental data (Sup. Fig. 3a) but with fixed known parameters (Sup. Fig. 3b) in an attempt to retrieve these values through the previously described fitting procedure. Estimates of MFI_{max}, K_D and SF could be retrieved with high accuracy across a range of artificial datasets with varied underlying parameters Sup. Fig. 3c-e).

Crystal structure analysis

Crystal structures of CD47 in complex with αhuman CD47 clone B6H12.2[53], a magrolimab diabody construct[54] and human SIRPα[34] were identified in the protein databank (PDB) with accession codes 5TZU, 5IWL and 2JJS, respectively. These were aligned to the CD47 monomers in UCSF ChimeraX[55]. Only the VH and VL domains are presented; for the magrolimab (Hu5F9-G4) diabody, the chains were hidden beyond the $(GGSGG)_2$ linkers. For TRP1 (PDB code 5M8L)[56], the N-terminal glutamine was replaced with a pGlu residue using Isolde[57], which fits the electron density map better than the glutamine residue originally modeled in.

TCGA data

RNA-seq data (RSEM quantified, batch normalized) was obtained from TCGA for 30 tumor types for QPCTL. Expression levels were plotted against tumor type using R statistics (v4.4.1) and ggplot2 (v3.5.1).

Statistical testing and reproducibility

Groups were compared in Graphpad Prism (V9.3.1 for Windows, San Diego, California USA, www.graphpad.com) using an Anova test or otherwise indicated in the text, and p-values lower than 0.05 were considered to be statistically significant. In general, experiments were conducted at least three times to obtain biological replicates as mentioned in the figure legends, and for flow cytometry analysis at least 100,000 live single cells were stained and 10,000 cells were measured and analyzed.

Reporting summary

Further information on research design is available in the Nature Portfolio Reporting Summary linked to this article.

Data availability

Hits of clinically relevant antibodies targeting proteins containing an N-terminal Q or E are provided in Supplemental Data 1. Data used for the main figures are provided in Supplemental Data 2.

Code availability

Code to estimate binding affinities from flow cytometry data and reproduced manuscript figures are available at: https://doi.org/10.5281/zenodo.16412041[58].

Received: 27 March 2025; Accepted: 24 September 2025;
Published online: 13 November 2025

References

1. Lu, R.-M. et al. Development of therapeutic antibodies for the treatment of diseases. *J. Biomed. Sci.* **27** (2020). https://doi.org/10.1186/s12929-019-0592-z
2. Willingham, S. B. et al. The CD47-signal regulatory protein alpha (SIRPa) interaction is a therapeutic target for human solid tumors. *Proc. Natl Acad. Sci.* **109**, 6662–6667 (2012).
3. Chao, M. P. et al. Anti-CD47 antibody synergizes with rituximab to promote phagocytosis and eradicate non-Hodgkin lymphoma. *Cell* **142**, 699–713 (2010).
4. Adams, S. et al. Signal-regulatory protein is selectively expressed by myeloid and neuronal cells. *J. Immunol.* **161**, 1853–1859 (1998).
5. Hendriks, M. A. J. M. et al. Bispecific antibody approach for EGFR-directed blockade of the CD47-SIRPα "don't eat me" immune checkpoint promotes neutrophil-mediated trogoptosis and enhances antigen cross-presentation. *OncoImmunology* **9**, 1824323 (2020).
6. Matlung, H. L. et al. Neutrophils kill antibody-opsonized cancer cells by trogoptosis. *Cell Rep.* **23**, 3946–3959. e3946 (2018).
7. Advani, R. et al. CD47 Blockade by Hu5F9-G4 and Rituximab in Non-Hodgkin's Lymphoma. *N. Engl. J. Med.* **379**, 1711–1721 (2018).
8. Sikic, B. I. et al. First-in-Human, First-in-Class Phase I Trial of the Anti-CD47 Antibody Hu5F9-G4 in Patients With Advanced Cancers. *J. Clin. Oncol.* **37**, 946–953 (2019).
9. Takechi, Y., Hara, I., Naftzger, C., Xu, Y. & Houghton, A. N. A melanosomal membrane protein is a cell surface target for melanoma therapy. *Clin. Cancer Res.: Off. J. Am. Assoc. Cancer Res.* **2**, 1837–1842 (1996).
10. Patel, D. et al. Generation and characterization of a therapeutic human antibody to melanoma antigen TYRP1. *Hum. antibodies* **16**, 127–136 (2007).
11. Jilani, S. et al. CAR-T cell therapy targeting surface expression of TYRP1 to treat cutaneous and rare melanoma subtypes. *Nat. Commun.* **15** (2024). https://doi.org/10.1038/s41467-024-45221-2
12. Spreafico, A. et al. Phase 1, first-in-human study of TYRP1-TCB (RO7293583), a novel TYRP1-targeting CD3 T-cell engager, in metastatic melanoma: active drug monitoring to assess the impact of immune response on drug exposure. *Front. Oncol.* **14** (2024). https://doi.org/10.3389/fonc.2024.1346502
13. Khalil, D. N. et al. An Open-Label, Dose–Escalation Phase I Study of Anti-TYRP1 Monoclonal Antibody IMC-20D7S for Patients with Relapsed or Refractory Melanoma. *Clin. Cancer Res.* **22**, 5204–5210 (2016).
14. Middelburg, J. et al. T-cell stimulating vaccines empower CD3 bispecific antibody therapy in solid tumors. *Nat. Commun.* **15** (2024). https://doi.org/10.1038/s41467-023-44308-6
15. Li, C.-W. et al. Eradication of triple-negative breast cancer cells by targeting glycosylated PD-L1. *Cancer cell* **33**, 187–201. e110 (2018).

16. Li, C.-W. et al. Glycosylation and stabilization of programmed death ligand-1 suppresses T-cell activity. *Nat. Commun.* **7**, 12632 (2016).
17. Sun, L. et al. Targeting Glycosylated PD-1 Induces Potent Antitumor Immunity. *Cancer Res.* **80**, 2298–2310 (2020).
18. Lee, T.-A. et al. Post-translational Modification of PD-1: Potential Pathways for Cancer Immunotherapy. *Cancer Res.* (2024). https://doi.org/10.1158/0008-5472.can-23-2664
19. Chu, C.-W. et al. Variable PD-1 glycosylation modulates the activity of immune checkpoint inhibitors. *Life Sci. Alliance* **7**, e202302368 (2024).
20. Lu, D. et al. PD-1 N58-Glycosylation-Dependent Binding of Monoclonal Antibody Cemiplimab for Immune Checkpoint Therapy. *Front. Immunol.* **13** (2022).
21. Liu, K. et al. N-glycosylation of PD-1 promotes binding of camrelizumab. *EMBO Rep.* **21**, e51444 (2020).
22. Wang, M. et al. Identification of a monoclonal antibody that targets PD-1 in a manner requiring PD-1 Asn58 glycosylation. *Commun. Biol.* **2**, 392 (2019).
23. Liu, J. et al. Study of the interactions of a novel monoclonal antibody, mAb059c, with the hPD-1 receptor. *Sci. Rep.* **9** (2019). https://doi.org/10.1038/s41598-019-54231-w
24. Cynis, H. et al. Isolation of an isoenzyme of human glutaminyl cyclase: retention in the Golgi complex suggests involvement in the protein maturation machinery. *J. Mol. Biol.* **379**, 966–980 (2008).
25. Zhang, Y. et al. Glutaminyl cyclases, the potential targets of cancer and neurodegenerative diseases. *Eur. J. Pharmacol*. 175178 (2022).
26. Liu, Y. E., Shi, Y. & Wang, P. Functions of glutaminyl cyclase and its isoform in diseases. *Vis. cancer med.* **4**, 1 (2023).
27. Barreira Da Silva, R. et al. *Loss of the intracellular enzyme QPCTL limits chemokine function and reshapes myeloid infiltration to augment tumor immunity* (Cold Spring Harbor Laboratory, 2022).
28. Wu, Z. et al. Unsynchronized butyrophilin molecules dictate cancer cell evasion of Vγ9Vδ2 T-cell killing. *Cell. Mol. Immunol.* (2024). https://doi.org/10.1038/s41423-024-01135-z
29. Mair, B. et al. High-throughput genome-wide phenotypic screening via immunomagnetic cell sorting. *Nat. Biomed. Eng.* **3**, 796–805 (2019).
30. Wu, Z. et al. Identification of Glutaminyl Cyclase isoenzyme isoQC as a regulator of SIRPα-CD47 axis. *Cell Res.* **29**, 502–505 (2019).
31. Logtenberg, M. E. W. et al. Glutaminyl cyclase is an enzymatic modifier of the CD47- SIRPα axis and a target for cancer immunotherapy. *Nat. Med.* **25**, 612–619 (2019).
32. Demattos, R. B. et al. A plaque-specific antibody clears existing beta-amyloid plaques in Alzheimer's disease mice. *Neuron* **76**, 908–920 (2012).
33. Raybould, M. I. J. et al. Thera-SAbDab: the Therapeutic Structural Antibody Database. *Nucleic Acids Res.* **48**, D383–D388 (2020).
34. Hatherley, D. et al. Paired Receptor Specificity Explained by Structures of Signal Regulatory Proteins Alone and Complexed with CD47. *Mol. Cell* **31**, 266–277 (2008).
35. Uhlen, M. et al. A pathology atlas of the human cancer transcriptome. *Science* **357**, eaan2507 (2017).
36. Bresser, K. et al. QPCTL regulates macrophage and monocyte abundance and inflammatory signatures in the tumor microenvironment. *OncoImmunology* **11** (2022). https://doi.org/10.1080/2162402x.2022.2049486
37. Labanieh, L. et al. Enhanced safety and efficacy of protease-regulated CAR-T cell receptors. *Cell* **185**, 1745–1763.e1722 (2022).
38. Wang, T. et al. Gentulizumab, a novel anti-CD47 antibody with potent antitumor activity and demonstrates a favorable safety profile. *J. Transl. Med.* **22** (2024). https://doi.org/10.1186/s12967-023-04710-6
39. Yang, H., Xun, Y. & You, H. The landscape overview of CD47-based immunotherapy for hematological malignancies. *Biomark. Res.* **11** (2023). https://doi.org/10.1186/s40364-023-00456-x
40. Sockolosky, J. T. et al. Durable antitumor responses to CD47 blockade require adaptive immune stimulation. *Proc. Natl Acad. Sci.* **113**, E2646–E2654 (2016).
41. Ingram, J. R. et al. Localized CD47 blockade enhances immunotherapy for murine melanoma. *Proc. Natl Acad. Sci.* **114**, 10184–10189 (2017).
42. Zhao, X. W. et al. CD47-signal regulatory protein- (SIRP) interactions form a barrier for antibody-mediated tumor cell destruction. *Proc. Natl Acad. Sci.* **108**, 18342–18347 (2011).
43. WHO. *World malaria report 2023*. (World Health Organization, 2023).
44. Dacon, C. et al. Protective antibodies target cryptic epitope unmasked by cleavage of malaria sporozoite protein. *Science* **387** (2025). https://doi.org/10.1126/science.adr0510
45. McCue, A. C. et al. Engineering a tumor-selective prodrug T-cell engager bispecific antibody for safer immunotherapy. *mAbs* **16** (2024). https://doi.org/10.1080/19420862.2024.2373325
46. Seifert, F. et al. Glutaminyl Cyclases Display Significant Catalytic Proficiency for Glutamyl Substrates. *Biochemistry* **48**, 11831–11833 (2009).
47. Richter, K., Kawashima, E., Egger, R. & Kreil, G. Biosynthesis of thyrotropin releasing hormone in the skin of Xenopus laevis: partial sequence of the precursor deduced from cloned cDNA. *EMBO J.* **3**, 617–621 (1984).
48. Yu, L. et al. Investigation of N-terminal glutamate cyclization of recombinant monoclonal antibody in formulation development. *J. Pharm. Biomed. Anal.* **42**, 455–463 (2006).
49. Benonisson, H. et al. CD3-Bispecific Antibody Therapy Turns Solid Tumors into Inflammatory Sites but Does Not Install Protective Memory. *Mol. Cancer Therapeutics* **18**, 312–322 (2019).
50. Diebolder, P. et al. Generation of "LYmph Node Derived Antibody Libraries" (LYNDAL) for selecting fully human antibody fragments with therapeutic potential. *mAbs* **6**, 130–142 (2014).
51. Van Antwerp, J. J. & Wittrup, K. D. Fine affinity discrimination by yeast surface display and flow cytometry. *Biotechnol. Prog.* **16**, 31–37 (2000).
52. Schuck, P. Use of surface plasmon resonance to probe the equilibrium and dynamic aspects of interactions between biological macromolecules. *Annu Rev. Biophys. Biomol. Struct.* **26**, 541–566 (1997).
53. Pietsch, E. C. et al. Anti-leukemic activity and tolerability of anti-human CD47 monoclonal antibodies. *Blood Cancer J.* **7**, e536–e536 (2017).
54. Weiskopf, K. et al. CD47-blocking immunotherapies stimulate macrophage-mediated destruction of small-cell lung cancer. *J. Clin. Investig.* **126**, 2610–2620 (2016).
55. Meng, E. C. et al. UCSF ChimeraX: Tools for structure building and analysis. *Protein Science* **32** (2023). https://doi.org/10.1002/pro.4792
56. Lai, X., Wichers, H. J., Soler-Lopez, M. & Dijkstra, B. W. Structure of Human Tyrosinase Related Protein 1 Reveals a Binuclear Zinc Active Site Important for Melanogenesis. *Angew. Chem. Int. Ed.* **56**, 9812–9815 (2017).
57. Croll, T. I. ISOLDE: a physically realistic environment for model building into low-resolution electron-density maps. *Acta Crystallogr. Sect. D. Struct. Biol.* **74**, 519–530 (2018).
58. *Depository Code for modeling*: https://doi.org/10.5281/zenodo.16412041, 2025).

Acknowledgements

The results shown in Fig. 6 are based upon data generated by the TCGA Research Network: https://www.cancer.gov/tcga. We thank the Leiden University Medical Center Flow Cytometry Facility for their support and cell sorting. This work was supported by a KWF grant and an NWO starters grant to F.A.S.

Author contributions

Conceptualization; A.v.d.P-v.D., L.M.T.W., J.B.B., F.A.S.; Methodology, A.v.d.P-v.D., L.M.T.W., C.L., M.v.D., I.D., J.B.B., F.A.S.; Investigation and

Validation. A.v.d.P-v.D., L.M.T.W., C.L., M.v.D., I.D., J.M.F.v.V., M.S., R.C.S., T.H.S., K.B.; Writing - original draft, A.v.d.P-v.D., L.M.T.W., J.B.B., F.A.S.; Writing– Review & Editing, A.v.d.P-v.D., L.M.T.W., C.L., M.v.D., I.D., J.M.F.v.V., G.S., M.S., T.J.B.v.G., R.v.D., T.v.H., R.C.S., T.H.S. J.B.B., K.B., F.A.S.; Funding Acquisition, F.A.S.; Resources, G.S., T.J.B.v.G., R.v.D., T.v.H.; Supervision, A.v.d.P-v.D., J.B.B., F.A.S.

Competing interests
The authors declare no competing interests.

Additional information
Supplementary information The online version contains supplementary material available at https://doi.org/10.1038/s42003-025-08938-4.

Correspondence and requests for materials should be addressed to Ferenc. A. Scheeren.

Peer review information *Communications Biology* thanks the anonymous reviewers for their contribution to the peer review of this work. Primary Handling Editors: Theam Soon Lim and Laura Rodriguez. A peer review file is available.